Progress in Natural Science: Materials International 2012;22(6):644–653

Chinese Materials Research Society

Progress in Natural Science: Materials International

www.elsevier.com/locate/pnsmi
www.sciencedirect.com

ORIGINAL RESEARCH

Photocatalytic degradation of benzene in gas phase by nanostructured $BiPO_4$ catalysts

Baihua Long[a], Jianhui Huang[a,b], Xinchen Wang[a,*]

[a]*Research Institute of Photocatalysis, State Key Laboratory Breeding Base of Photocatalysis, Fuzhou University, Fuzhou 350002, PR China*
[b]*Department of Environment and Life Sciences, Putian University, Putian 351100, PR China*

Received 25 July 2012; accepted 7 October 2012
Available online 21 December 2012

KEYWORDS

Photocatalyst;
$BiPO_4$;
Environmental purification

Abstract A rod-shaped $BiPO_4$ photocatalyst was prepared by a simple hydrothermal method for light-induced catalytic degradation of stable aromatic compounds such as benzene in gas phase under ambient conditions. The samples were subjected to various technical characterizations including X-ray diffraction (XRD), transmission electron microscopy (TEM), UV/vis and FTIR spectrum, to determine the crystal structure, morphology, and optical properties of the as-prepared photocatalysts. Results indicate that $BiPO_4$ exhibits much higher photocatalytic activity and stability under UV light irradiation than that of commercial TiO_2 (Degussa P25) in the degradation of benzene to CO_2. The active radical species involved in the degradation reactions over $BiPO_4$ photocatalyst have been investigated by the spin-trapping electron paramagnetic resonance (EPR) spectra and a photoluminescence technique. Theoretical calculations reveal that $BiPO_4$ contains highly-dispersive conduction bands, enabling high mobility of the photo-generated carries and therefore leading to fast charge transfer and separation.

1. Introduction

Benzene is a toxic chemical that occurs naturally in the environment but is used by human in a wide range of products such as mucilage, paints, plastics, rubber and gasoline. Therefore, benzene is an important pollutant in the urban and indoor air. It is already confirmed that exposure to benzene for a long-time or at high levels can result in a number of ailments including drowsiness, dizziness, headache, lightheadedness, nausea and even cancers. Thus, this chemical has been

*Corresponding author. Fax: +86 591 83738608.
E-mail address: xcwang@fzu.edu.cn (X. Wang).

Peer review under responsibility of Chinese Materials Research Society.

ELSEVIER Production and hosting by Elsevier

1002-0071 © 2012 Chinese Materials Research Society. Production and hosting by Elsevier Ltd. All rights reserved.
http://dx.doi.org/10.1016/j.pnsc.2012.11.007

classified as a class A carcinogenic by the Environmental Protection Agency [1,2]. Many technologies such as thermal incineration, catalytic incineration [3,4], oxidation with ozone or supercritical water [5,6], degradation using a plasma-based system [7] have been developed for completely removing benzene from the air. Unfortunately, most of these technologies are not efficient and economic in treating benzene at low concentrations, for examples at ppb or ppm level.

Photocatalytic oxidation of benzene and other aromatic compounds at low levels over titanium dioxide (TiO_2) has been examined by several research groups [8–10]. Although its photocatalytic oxidation has proven to be effective, continuous-flow photocatalytic reactors for the treatment of gas-phase aromatics generally yield moderate conversion only. In addition, the fast and apparent catalyst deactivation typically occurred during the operation. Recently, our group and others have reported that some non-TiO_2 photocatalysts such as Ga_2O_3, InOOH, $Sr_2Sb_2O_7$, Zn_2GeO_4, $ZnGa_2O_4$, and $Cd_2Ge_2O_6$ can catalyze the efficient degradation of benzene under UV irradiation to CO_2 and water. The main feature of these kind of metal oxide photocatalysts in the treatment of benzene is that they did not suffer from a significant catalytic deactivation during prolonged reaction time [11–16] due to their high redox potentials associated with the wide band gap. This is distinctly different from the TiO_2 photocatalysts that are susceptible to surface carbonization during treatment of benzene. The carbonization blocks the surface active sites of TiO_2 and thereafter passivates and deactivates TiO_2 photocatalysts, irreversibly. Despite the high stability of these materials, these new metal oxide photocatalysts are composed of metal components such as Ga, In, Ge and Sb that are too rare and expensive to be used broadly. Thus, it calls for the design and development of more powerful and durable photocatalysts for the treatment of benzene.

There are a large number of nonmetal salts based semiconductors such as phosphates, sulphates in the nature which is much cheaper than precious metal oxide or precious metal salts, allowing their practical applications in industry. For example, Zhu and his coworkers [17–22] reported that $BiPO_4$ shows improved photocatalytic activity for the degradation of organic pollutants in aqueous phase over commercial TiO_2 (P25). So far, it remains unknown whether $BiPO_4$ catalyst can act as an effective and stable photocatalyst towards the degradation of volatile organic compounds including benzene in the gas phase. This motivates us to explore the potential applications of $BiPO_4$ for the degradation benzene in the air under ambient conditions, without applying co-catalysts.

In the present study, we applied a simple hydrothermal method to fabrication nanostructued $BiPO_4$ for the treatment of benzene in gas phase. The prepared materials were fully characterized by XRD, TEM, UV/vis, and FTIR techniques. The study results demonstrated that photocatalytical activity of $BiPO_4$ is much higher than that of commercial TiO_2 (P25) for the decomposition of benzene under the same experimental conditions. In addition, our investigations also demonstrated that the post-calcined treatment of $BiPO_4$ can further enhance the photocatalytic activity of $BiPO_4$ photocatalysts. The electronic band structure of $BiPO_4$ was therefore investigated to reveal the physical insights accounting for its high photocatalytic activity in the treatment of stable benzene molecules. The photoactive radical species involved in the degradation reaction were also described.

2. Experimental

2.1. Catalyst preparation

All of the reagents were analytically pure and without further purification before used. $BiPO_4$ was synthesized by a hydrothermal method. In a typical synthesis, 3.88 g $Bi(NO_3)_3 \cdot 5H_2O$ was added to 75 mL of phosphoric acid (1 mol/L) with strongly magnetic stirring at room temperature. The resulting mixture was stirred for 1 h and then transferred to a 100 mL stainless telflon-lined autoclave. The autoclave was maintained at 160 °C for 12 h under autogenous pressure, followed by cooling naturally to room temperature. After centrifugation, washing and drying, the resulting sample was denoted as $BiPO_4$-160. The above-mentioned $BiPO_4$-160 was further calcined at 750 °C in air for 2 h to obtain the heat-treated sample denoted as $BiPO_4$-750.

2.2. Characterization

The phase composition of the samples was determined by X-ray diffraction (XRD) on a Bruker D8 Advance X-ray diffractometer at 40 kV and 40 mA with Ni-filtered Cu Kα radiation. Transmission electron microscopy (TEM) characterizations were collected on a JEOL model 2010 EX instrument operating at an accelerating voltage of 200 KV, to which an energy dispersive X-ray emission analyzer (EDX) was attached. Nitrogen sorption experiments were carried out at 77 K by using the Micromeritics ASAP 2020 equipment. The optical properties were analyzed by UV–vis diffuse reflectance using a UV–vis spectrophotometer (Cary-500, Varian Co.) equipped with an integrating sphere attachment. FTIR spectra were recorded on a Nicolet Nexus 670 FTIR spectrometer at a resolution of 4 cm^{-1}. X-ray photoelectron spectroscope analysis was conducted on an ESCA lab250 photoelectron spectrometer (thermo Fisher Scientific) by using monochromatic Al *K*α X-ray beam as the excitation source and all binding energies were calibrated by the C 1 s peak of the surface adventitious carbon at 284.6 eV. The photoluminescence (PL) excitation and emission spectra were taken on a FL/FS 900 time-resolved fluorescence spectrometer. Electron spin resonance spectra were obtained using a Bruker model A300 instrument with a 200 W mercury–xenon lamp with a wavelength centered at 254 nm as irradiation light source. The band structure and density of states (DOS) calculations were performed by using the CASTEP program belonging to a DFT plane-wave pseudopotential method. The flat-band potentials (V_{fb}) of $BiPO_4$ were determined from Mott–Schottky plots by electrochemical method, which was carried out in conventional three electrode cell using a Zenuium electrochemical workstation (Zahner Co.).

2.3. Photocatalytic activity measurement

The gas-phase photocatalytic degradation of benzene was conducted with a fixed bed tubular quartz reactor operated in a continuous-flow mode. The weights of the catalysts were 0.3 g, with a particle size of 0.21–0.25 mm. The light source was provided by four 4 W UV lamps with a wavelength centered at 254 nm (Philips, TUV4W/G4 T5). A bubbler that contained benzene was immersed in an ice-water bath and

benzene (about 300 ppm) bubbled with oxygen from the gas cylinder was fed to the catalyst at a total flow rate of 20 mL/min. The reaction temperature was controlled at 30 ± 1 °C by an air-cooling system. The analysis of the reactor effluent was conducted by a gas chromatograph (HP6890) equipped with a flame ionization detector, a thermal conductivity detector, and a Porapak R column. The benzene was found to be stable in the reactor without illumination, and no degradation was observed when the benzene was illuminated in the absence of catalyst. Conversion and mineralization of benzene were defined as the following:

$$\text{conversion} = \left[\frac{Co - C}{Co}\right] \times 100\%$$

$$\text{mineralization} = \left[\frac{(CO_2)\text{produced}}{6(\text{benzene})\text{converted}}\right] \times 100\%$$

where Co is the initial concentration of benzene and C is the concentration of benzene after the photocatalytic reaction.

3. Results and discussion

The phase structure of the as-prepared sample has been analyzed by the XRD technique. Fig. 1 shows the XRD patterns of the $BiPO_4$-160 sample synthesized by the hydrothermal approach and the $BiPO_4$-750 sample obtained by post-calcined treatment at 750 °C for 2 h. XRD patterns can be indexed to a pure monoclinic phase of well-crystallized $BiPO_4$, well consistent with the reported data (JPCDS 80-0209). The peaks at 2θ values of 19.01°, 21.31°, 27.13°, 29.04°, and 31.16° match well with the (011), ($\bar{1}$11), (200), (120), and (012) crystal planes of $BiPO_4$, respectively. There is no any trace of impurity phase under the instrument's resolution, indicating the high purity and high crystallinity of the samples. The post-calcined $BiPO_4$-750 sample shows the intensity of the highest peaks slightly sharper than that of $BiPO_4$-160, indicating the formation of better crystallites in the $BiPO_4$-750 sample. The average crystallite sizes of the samples are calculated by the Scherrer equation are estimated to be 74 nm and 80 nm for $BiPO_4$-160 and $BiPO_4$-750, respectively.

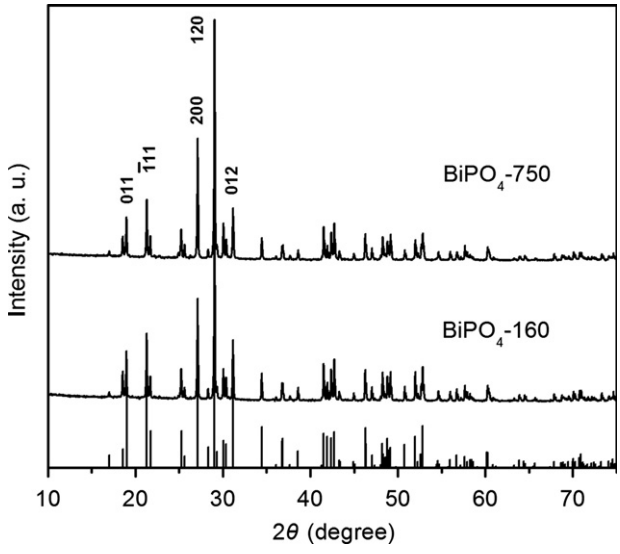

Fig. 1 XRD patterns of the $BiPO_4$-160 and $BiPO_4$-750.

The morphology of the as-synthesized $BiPO_4$-750 was analyzed by TEM, as shown in Fig. 2a. It can be clearly seen that the $BiPO_4$-750 sample consists of a large quantity of irregular rods with 300 nm–2 μm in length and 100 nm–300 nm in width, but with tiny particles around them. The high-resolution TEM image (Fig. 2b) shows the resolved lattice spacing of $d = 0.47$ nm, corresponding well to the (011) crystallographic plane of monoclinic $BiPO_4$. The chemical composition of the $BiPO_4$-750 sample was further characterized by energy dispersive X-ray spectroscopy (EDS), and the results (Fig. 2c) confirmed that except for the elements Cu and C from the copper wafer, the as-prepared photocatalysts were composed of Bi, P, and O, only.

The assessment of the surface elemental composition and oxidation state of the sample was studied by XPS analysis. Fig. 3a is the XPS survey spectrum of $BiPO_4$-750 which contains the peaks of Bi 4f, Bi 4d, O 1s, P 2s, P 2p and C 1s. The C element can be ascribed to the adventitious hydrocarbon from the XPS instrument itself. The high-resolution XPS spectra of the Bi 4f, P 2p and O 1s region on the surface of the sample are shown in Fig. 3b–d. Two typical peaks of Bi 4f located at about 164.9 eV and 159.6 eV can be assigned to the binding energies of Bi 4 $f_{5/2}$ and Bi 4f $_{7/2}$ (Fig. 3b), respectively [23]. This indicates the existence of a trivalent oxidation state for bismuth. The XPS spectra in P 2p region exhibit a broad signal peaking at around 132.8 eV, as shown in Fig. 3c. The binding energy of 132.8 eV suggests that the P in the sample exist in the oxidation state of P^{5+}. In Fig. 3d, the O may be fitted to two kinds of chemical states: crystal lattice oxygen and adsorbed oxygen. The peak at 530.8 eV is assigned to the crystal lattice oxygen, while the peak at 532.5 eV is related to adsorbed oxygen. The chemical composition of the sample was calculated using the relative sensitivity factors. The result suggested that the molar ratio of Bi:P:O are 1:1.26:3.66, which approach the expected stoichiometry of $BiPO_4$.

Optical absorption of the as-synthesized $BiPO_4$ samples was measured by UV/visible spectrometer, as shown in Fig. 4. The optical transition in the $BiPO_4$ is indirectly allowed, in accordance with the later theoretical calculation, where the $BiPO_4$ catalyst is demonstrated to an indirect semiconductor. The sample presents absorption edge around 281 nm, corresponding to the band gap energy of 4.4 eV.

The gas phase photocatalytic decomposition of benzene in a dry O_2 stream was carried out under ambient temperature and pressure. Reference experiments shows that no photocatalytic activity is observed in the absence of catalyst or light irradiation, thus confirming that the photodegradation reaction is really enabled by a photocatalytic process. Fig. 5a,b displays the photocatalytic conversion of benzene and the concentration of produced CO_2 over $BiPO_4$-160, and $BiPO_4$-750 photocatalysts as a function of reaction time, together with TiO_2 data as a comparison. The photocatalytic activity of $BiPO_4$-160 (conversion rate,~8%) and $BiPO_4$-750 (conversion rate, ~16%) for benzene photodegradation exhibited ~2 and~4 times higher conversion than that of P25 (conversion rate, 4%), respectively. This result reveals that the $BiPO_4$ has much higher photocatalytic activity than that of TiO_2. And the post-calcined treatment could enhance noticeably the photocatalytic activity toward the benzene degradation, which

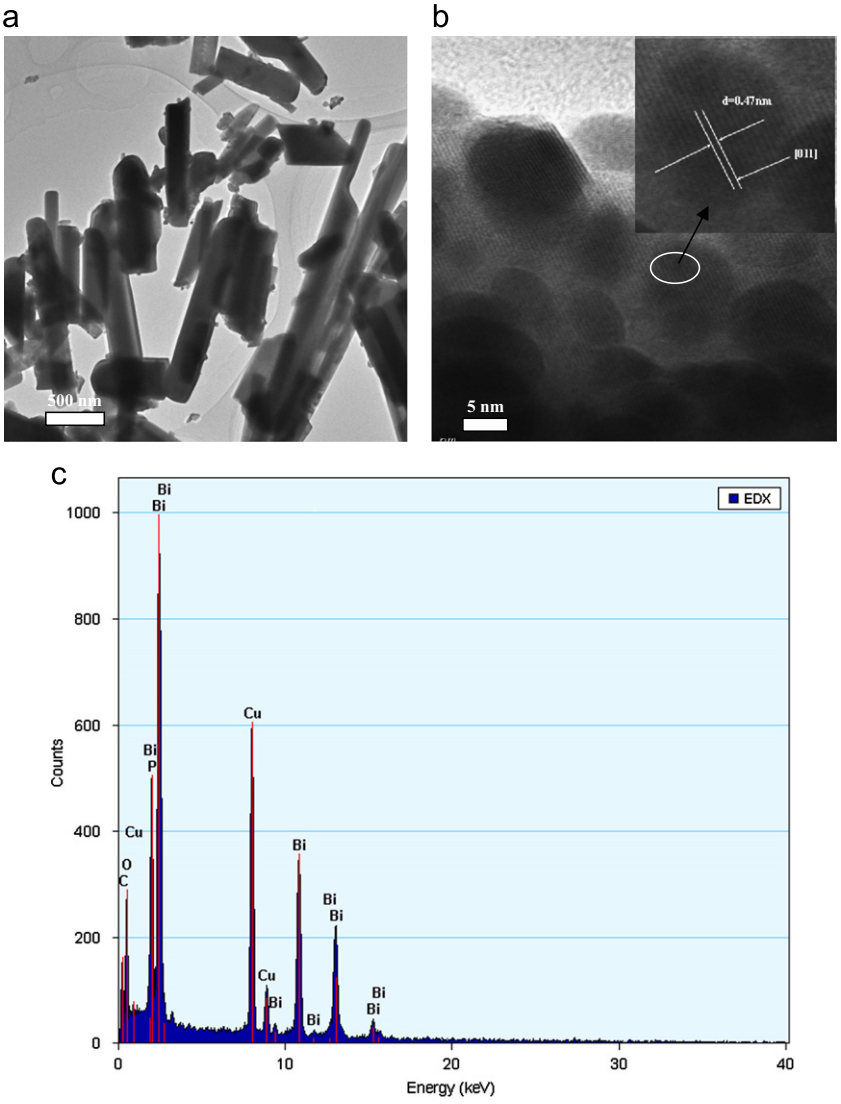

Fig. 2 TEM images and EDS spectrum of $BiPO_4$-750: (a) Image at low magnification; (b) HRTEM image; (c) EDS spectrum.

may be due to the removal of some impurities absorbed on the surface of sample and the increased crystalline caused by the post-thermal annealing at 750 °C. The measurement of maximum CO_2 produced (145 ppm) from the $BiPO_4$-750 photocatalyst also confirms the beneficial effect of post-thermal treatment. The corresponded mineralization ration of 52% was calculated for the system, where small amount of CO to balance carbon for the reaction. The formation of CO was indeed detected by in-situ FTIR spectroscopy as shown by the gradual increase in intensity of the CO bands in the region of 2300–2100 cm^{-1} in Fig. 5e,f. To demonstrate that $BiPO_4$-750 is an excellent photocatalyst with a high catalytic stability, the long-time operation of the photocatalytic reaction over $BiPO_4$-750 with P25 photocatalyst was compared. Results illustrated in Fig. 5c,d show that P25 possesses a poor activity as indicated by the low initial conversion of ~4%, which decreased gradually to lower than 1% after 80 h reaction, accompanying with the production of small quantities of CO_2 (13 ppm). The color of the P25 catalyst turned from white to black after the prolonged reaction, well observed for TiO_2 photocatalyst in the treatment of benzene [11]. This is mainly due to the deposition of the intermediates on the surface of P25 surface during the reaction. However, for $BiPO_4$-750 photocatalyst, the reaction rate did not decrease noticeably during 110 h of reaction, reflecting the high photostability of $BiPO_4$-750 for the degradation of benzene. In addition, the conversion of benzene was nearly negligible when the light was turned off and was resumed immediately at about the same rate when the light was turned on again. These results provided an extra confirmation that the reaction really proceeded via photocatalysis.

To test whether the physicochemical properties of the used $BiPO_4$-750 photocatalyst change or not, further characterizations (XRD and XPS) have been performed on the sample before or after the photodegradation reaction. XRD (Fig. 6) showed that there was no observable change in the crystal structure between the sample before and after the reaction, suggesting the stability of the crystal phase under prolonged exposure to the deep UV irradiation. There was also no noticeable change in XPS spectra (Fig. 7), indicating high chemical stability of the samples in the photocatalytic process.

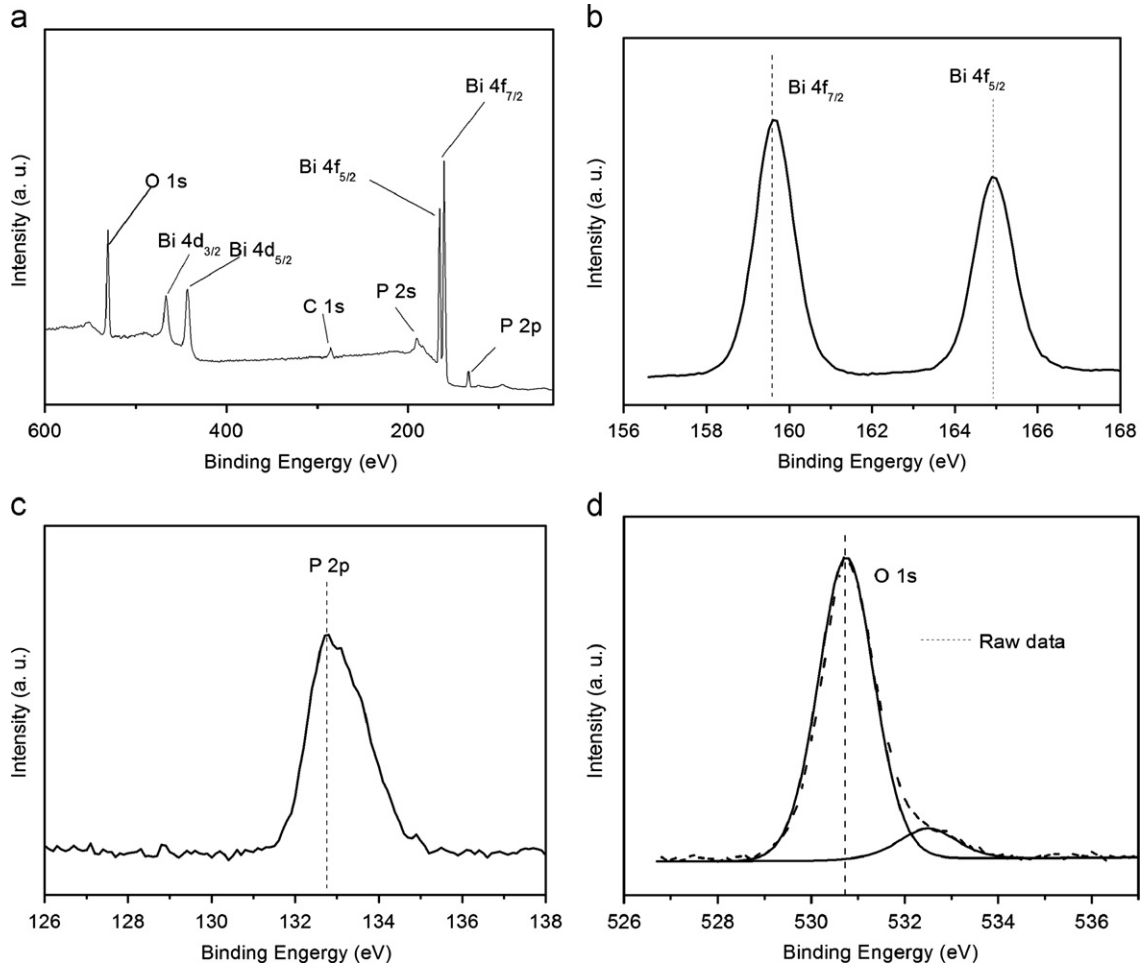

Fig. 3 The XPS survey spectrum and the high- resolution XPS spectra of $BiPO_4$-750 sample.

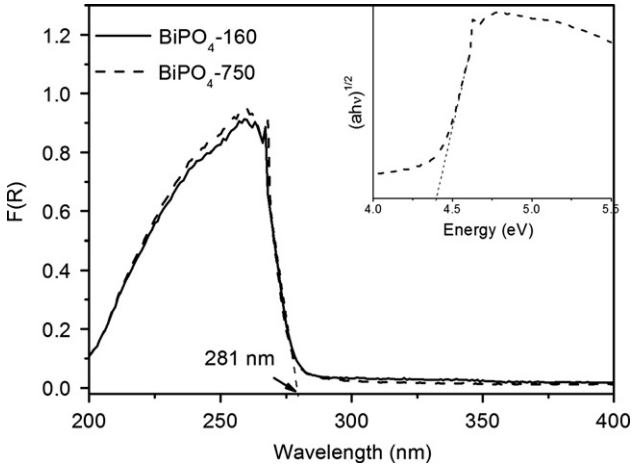

Fig. 4 Diffuse absorption coefficient F(R) of $BiPO_4$-160 and $BiPO_4$-750 samples. The inset is the optical band gap energy E_g of $BiPO_4$-750.

The above-mentioned results demonstrated that $BiPO_4$ has high stability in the photocatalytic application in the gas phase for the degradation of aromatic benzene in the air.

It is well-known that photocatalytic activity of a semiconductor is closely related to its band structure. The DFT method was therefore carried out to determine the electronic structures of $BiPO_4$, and its band structure and density of states (DOS) is displayed in Fig. 8a,b. The Fermi level indicated by dashed line is set as zero. For $BiPO_4$ catalyst, an indirect transition from the valance band maximum at the point D to the conduction band minimum at the point E as the minimum band gap with a value of 3.91 eV is predicted. These results can be obtained as follows: an occupied band on the low-energy side consists of the O 2s, P 3s, and P 3p. The occupied band in the middle consists of the hybrid orbital of O 2p, P 3s, P 3p, Bi 6s and Bi 6p. The occupied band on the high-energy side, corresponding to the broad valence band, consists of only the O 2p orbitals. The lowest-unoccupied band mainly comprises the Bi 6p orbital, with a small contribution of the O 2p and P 3p, corresponding to conduction band. The partial DOS for $BiPO_4$ is also shown in Fig. 9. The Fermi level is set to zero on the abscissa. The highest-occupied molecular orbital (HOMO) shows the p orbital lobes on the O atom, indicating that the orbital is purely composed of the O 2p orbitals. The lowest-unoccupied molecular orbital (LUMO) is mainly formed by the Bi 6p orbital, but the O 2p and P 3p is included to some degree. This mixing is rather common for composite metal oxide semiconductors including

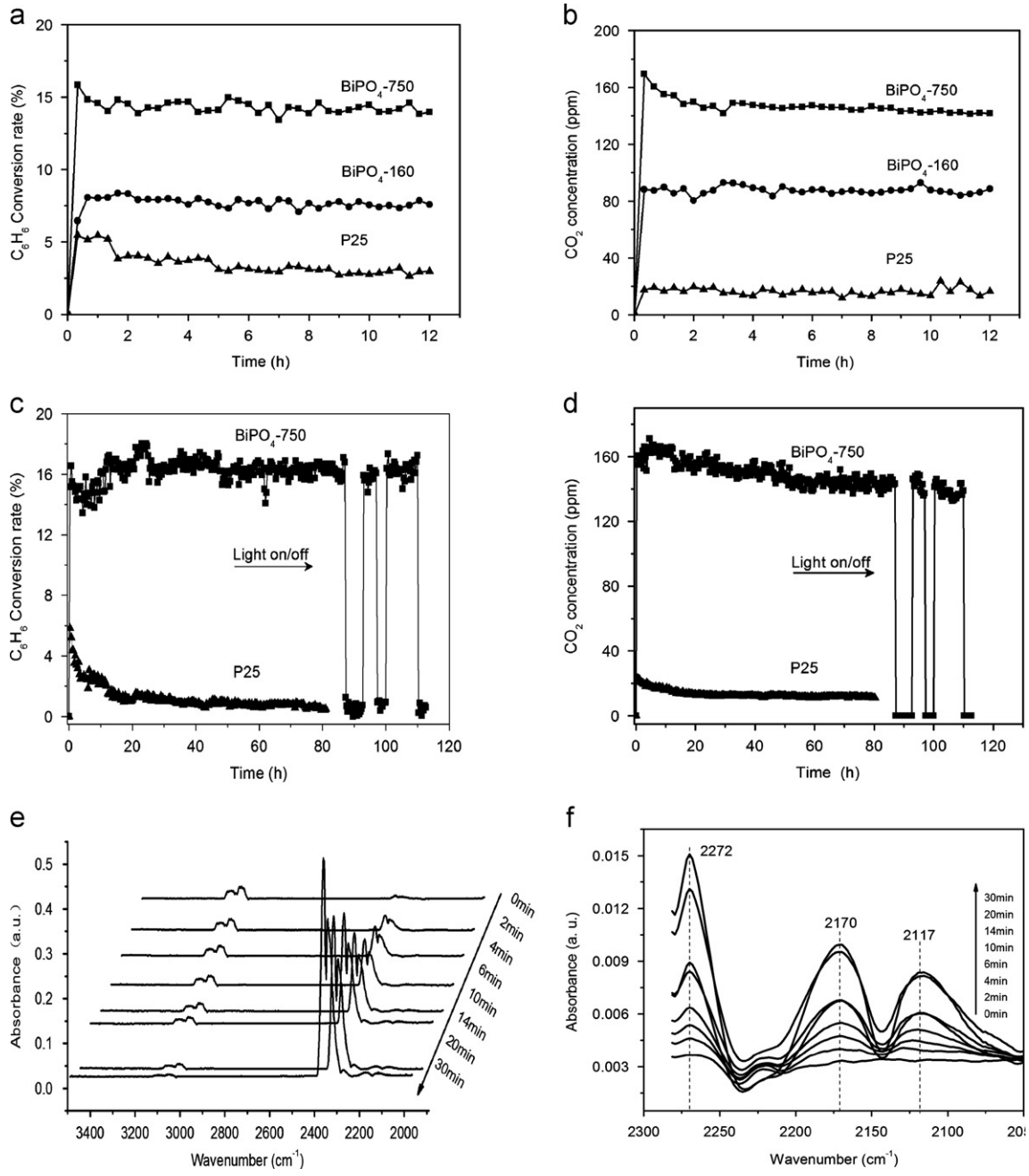

Fig. 5 (a) Photocatalytic conversion of benzene and (b) concentration of produced CO_2 in the stream over the $BiPO_4$-160 and $BiPO_4$-750 sample as a function of reaction time, with P25 as a reference. Stability test of $BiPO_4$-750 and P25 for conversion of benzene (c) and the product of CO_2 concentration (d) respectively. The FTIR of (e) $BiPO_4$-750 during the photodegradation benzene with irradiation time from 0 min to 30 min and (f) the bands of CO region as a function of irradiation time.

the d^{10} elements [24,25] and beneficial to larger dispersions of conduction bands which is good for the mobility of photo-generated carriers and lead to a higher separation efficiency of electron–hole pairs.

In the next set of experiments, we carried out electrochemical analysis of $BiPO_4$ to evaluate its electronic band structure. As shown in Fig. 10, the flat-band potential determined from Mott–Schottky plots is ca. −1.2 V vs. Ag/AgCl at pH 6.8 for $BiPO_4$ sample, corresponding to a potential of −1.1 V vs. NHE at pH 7. Moreover, it obviously seen that $BiPO_4$ has a characteristic behavior of a n-type semiconductor due to the positive slope of the liner plot. For n-type semiconductor, the conduction bands are very proximity to its flat-band potentials. Thus, by combining with the band gap estimated from optical absorption, the redox potentials of conduction band and valence band of $BiPO_4$ sample are −1.1 and 3.3 V NHE, respectively as shown in Scheme 1. This reveals that the photo-generated carries of

$BiPO_4$ have strong redox potentials in photocatalytic reaction. The photoexcited electrons in the conduction band possess a large thermodynamic driving force to reduce O_2 ($O_2/\cdot O_2^-$, −0.16 V vs. NHE), and the holes in the valence band can be captured by H_2O to give $\cdot OH$ radicals ($H_2O/\cdot OH$, 2.4 V vs. NHE). These species are known to be involved and played vital roles in the photocatalytic reaction.

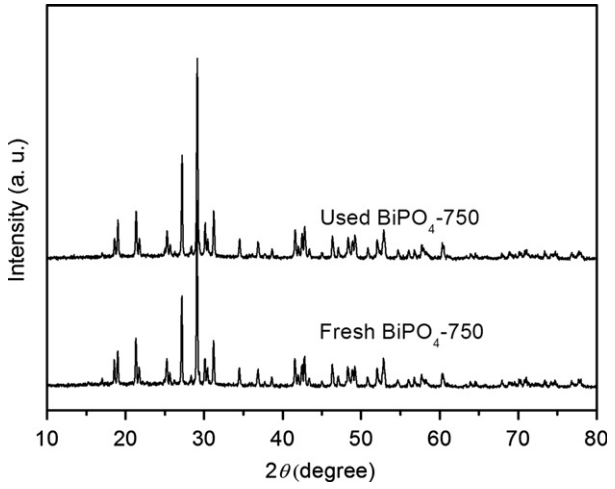

Fig. 6 XRD patterns of $BiPO_4$-750 before and after photodegradation of benzene.

To confirm the photoactive radical species with strong oxidation power for degradation of benzene over the $BiPO_4$ photocatalyst, the spin-trapping electron paramagnetic resonance (EPR) spectra has been used to detect the photogenerated radical species over $BiPO_4$ upon the irradiation of light, as shown in Fig. 11a,b. It can be seen clearly that the intensity of hydroxyl radicals and superoxide radicals over $BiPO_4$-750 sample under the UV light irradiation is much higher than that of $BiPO_4$-160 sample (Fig. 11a,b). This well explained the higher photocatalytic activity of $BiPO_4$-750 sample than that of $BiPO_4$-160 sample towards the degradation of benzene as described above. To further confirm the formation of $\cdot OH$ radicals, a terephthalic acid photoluminescence probing technique was also performed for the $BiPO_4$ photocatalytic systems. The insert of Fig. 11c shows the changes in the PL spectra in the terephthalic acid solutions with irradiation time over $BiPO_4$ photocatalysts. It is clear that the PL intensity at about 426 nm increases gradually with the irradiation time. The $\cdot OH$ radicals detected are proportional to the light irradiation time, which obeys zero-order reaction rate kinetics. As depicted in Fig. 11c, the formation rates of $\cdot OH$ radicals over $BiPO_4$-750 is much higher than that over $BiPO_4$-160, which is consistent with the EPR results. All these results provide direct proofs to explicate the enhanced photocatalytic

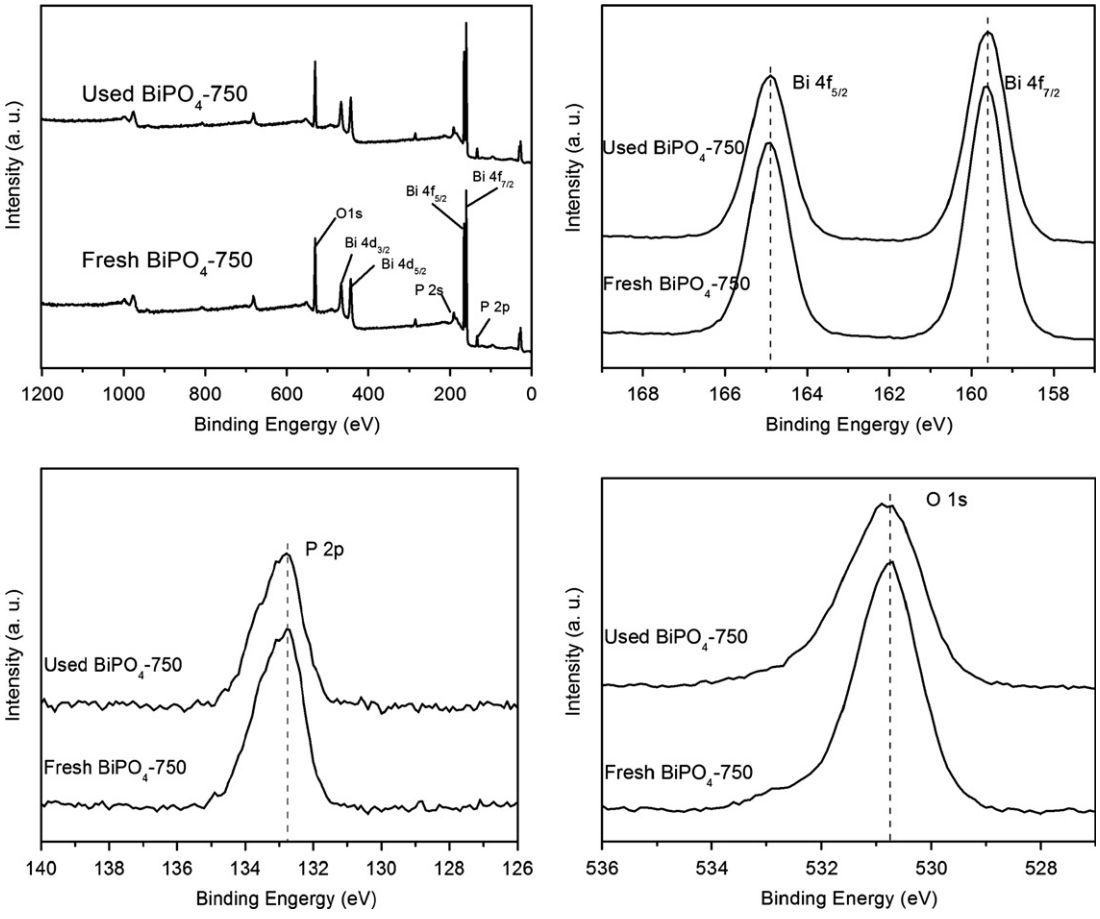

Fig. 7 High-resolution XPS spectra of $BiPO_4$-750 sample before and after photodegradation of benzene.

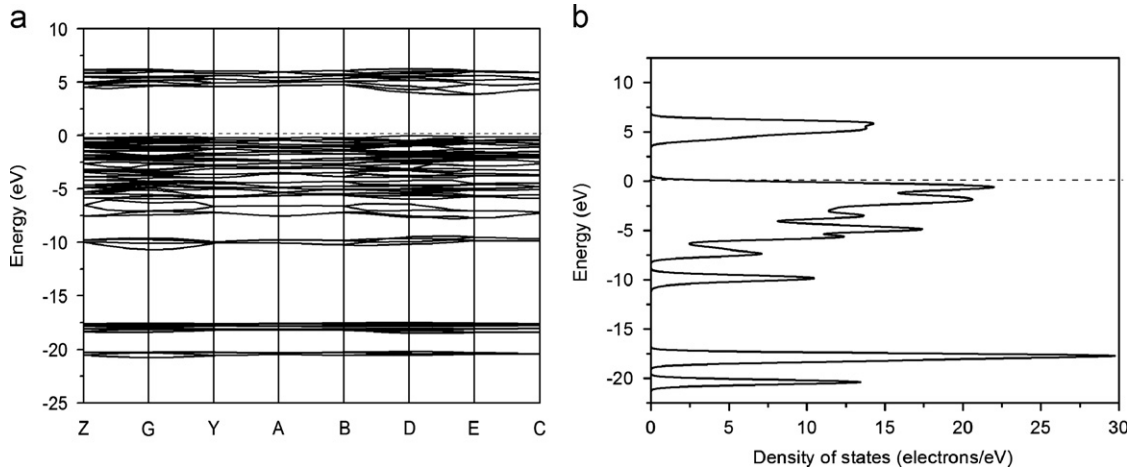

Fig. 8 DFT calculations for $BiPO_4$: (a) energy band dispersion; (b) density of states.

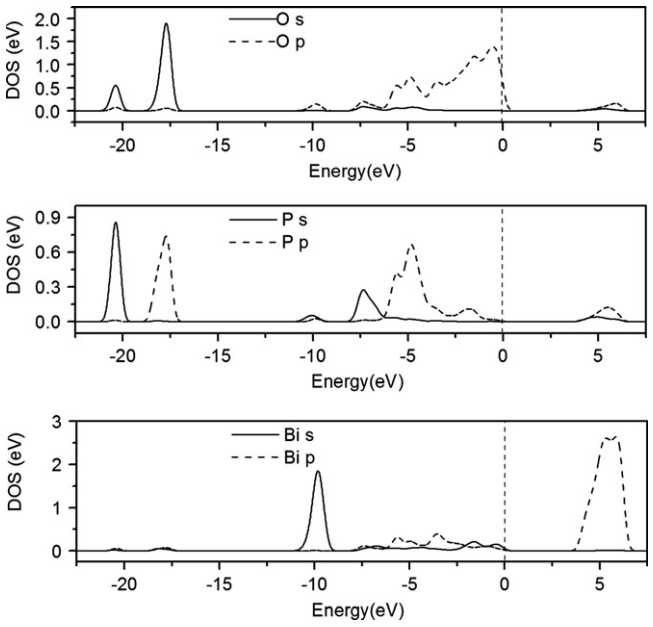

Fig. 9 The partial density of states for $BiPO_4$.

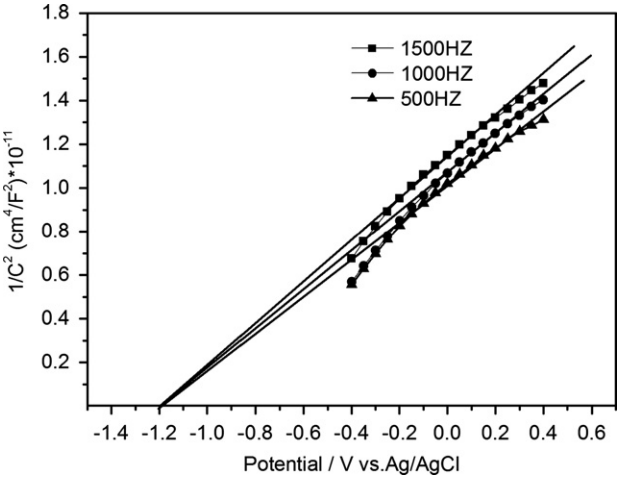

Fig. 10 Mott–Schottky plot for the $BiPO_4$ in 0.2 M Na_2SO_4 aqueous solution (pH = 6.8).

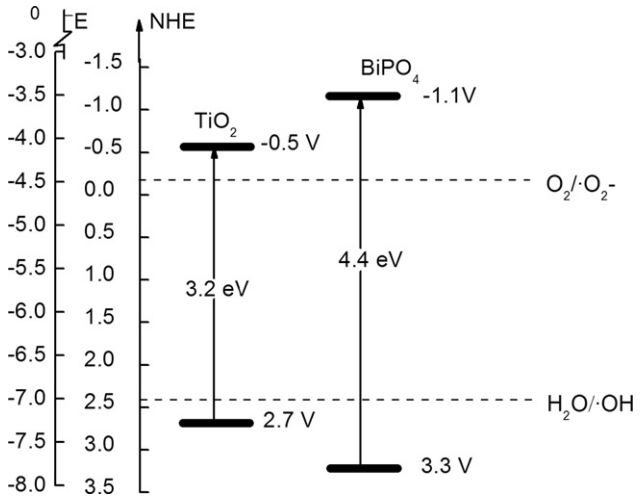

Scheme 1 Position of the energy levels of the conduction band edge (E_{CB}) and the valence band edge (E_{VB}) of TiO_2 and $BiPO_4$ with respect to the NHE.

activity of $BiPO_4$-750 over $BiPO_4$-160 in the photodegradation of benzene.

4. Conclusions

In conclusion, we have successfully demonstrated a facile route to prepare nanostructured $BiPO_4$ for the photodegradation of aromatic benzene, avoiding the use of high cost and rare metal of raw materials. The $BiPO_4$ sample exhibited remarkable improved activities and stabilities over P25 (50 m^2/g) towards photodegradation benzene, albeit with a low specific surface area of ~4 m^2/g. The post-thermal treatment of the sample has been demonstrated to further enhance the photocatalytic performance of $BiPO_4$. To make the sample more valuable for the photocatalysis, it is desired to create nanopores in the $BiPO_4$ framework, increasing its specific surface area for supporting gas–solid phase heterogeneous photocatalysis where mass transfer has been demonstrated to be rate limited step. Further studies will focus on the improvement of the texture of the materials by nano-

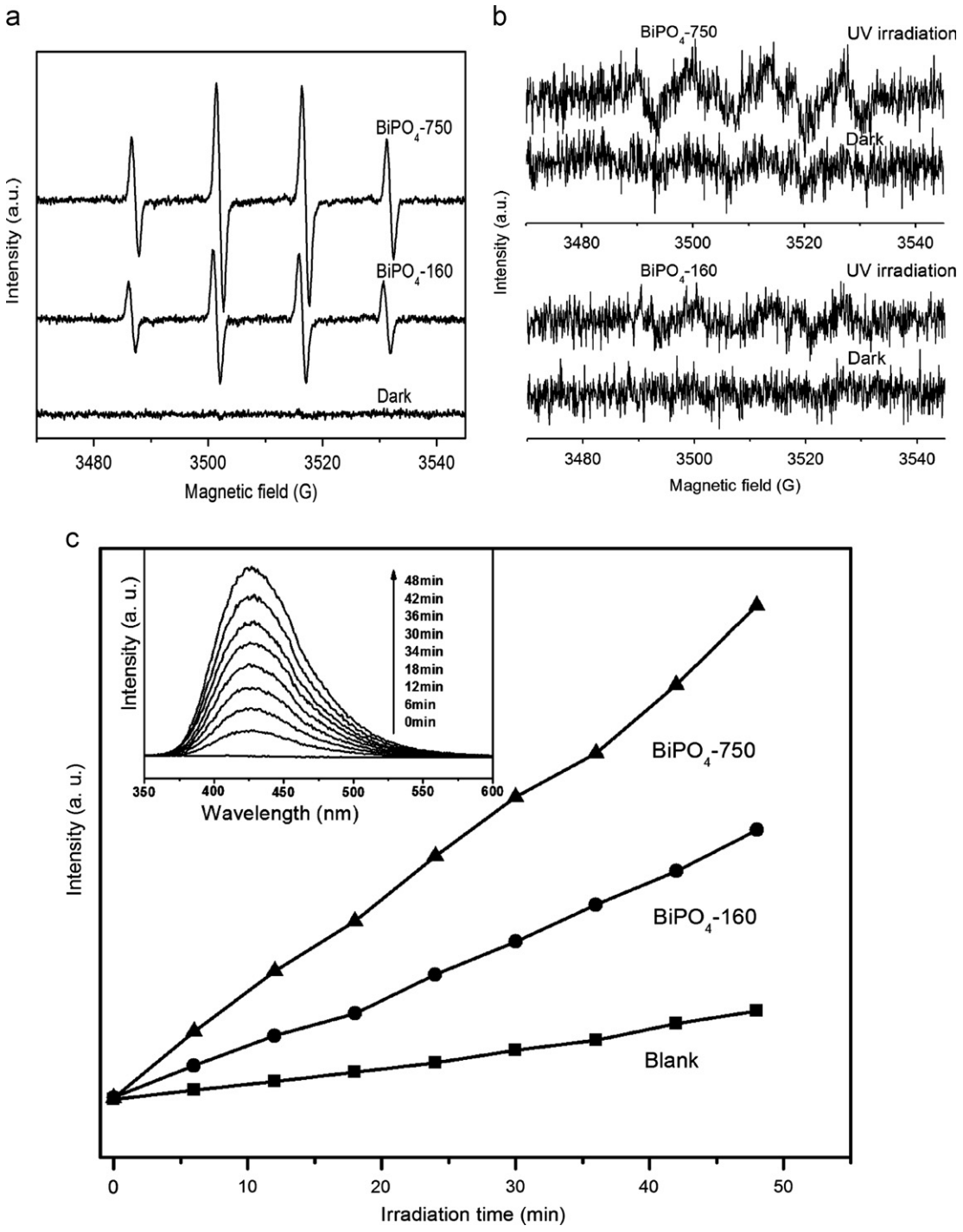

Fig. 11 ESR spectra of DMPO-OH (a) and DMPO-O_2^- (b) adducts in the system of $BiPO_4$-160 and $BiPO_4$-750 before and after light irradiation. (c) Plots of the induced fluorescence intensity at 426 nm against irradiation time for $BiPO_4$-160 and $BiPO_4$-750 samples. Inset: ·OH-trapping photoluminescence spectra of $BiPO_4$-750 sample in a solution of terephthalic acid at room temperature (excitation at 312 nm, emission at 426 nm).

structural design. These studies are currently underway in our laboratory.

Acknowledgments

This work was financially supported by the National Basic Research Program of China (Grant No. 2013CB632405) and the National Natural Science Foundation of China (Grant Nos. 21033003 and 21103095).

References

[1] Q. Lan, L.P. Zhang, G. Li, et al., Hematotoxicity in workers exposed to low levels of benzene, Science 306 (2004) 1774–1776.

[2] R.T.S. Oliveira, G.R. Salazar-Banda, M.C. Santos, et al., Electrochemical oxidation of benzene on boron-doped diamond electrodes, Chemosphere 66 (2007) 2152–2158.
[3] J.M. Padilla, G. Del Angel, J. Navarrete, Improved Pd/γ–Al_2O_3–Ce catalysts for benzene combustion, Catalysis Today 133–135 (2008) 541–547.
[4] D. Andreeva, P. Petrova, L. Ilieva, et al., Design of new gold catalysts supported on mechanochemically activated ceria–alumina, promoted by molybdena for complete benzene oxidation, Applied Catalysis B: Environmental 77 (2008) 364–372.
[5] J.L. Dinaro, J.B. Howard, W.H. Green, et al., Elementary reaction mechanism for benzene oxidation in supercritical water, The Journal of Physical Chemistry A 104 (2000) 10576–10586.
[6] H. Einaga, S. Futamura, Catalytic oxidation of benzene with ozone over alumina-supported manganese oxides, Journal of Catalysis 227 (2004) 304–312.
[7] C. Ratanatawanate, M. Macias, B.W.L. Jang, Promotion Effect of the nonthermal RF plasma treatment on Ni/Al_2O_3 for benzene hydrogenation, Industrial and Engineering Chemistry Research 44 (2005) 9868–9874.
[8] X.Z. Fu, W.A. Zeltner, M.A. Anderson, The gas-phase photocatalytic mineralization of benzene on porous titania-based catalysts, Applied Catalysis B: Environmental 6 (1995) 209–224.
[9] W.A. Jacoby, D.M. Blake, J.A. Penned, et al., Heterogeneous photocatalysis for control of volatile organic compounds in indoor air, Journal of the Air and Waste Management Association 46 (1996) 891–898.
[10] S. Sitkiewitz, A. Heller, Photocatalytic oxidation of benzene and stearic acid on sol–gel derived TiO_2 thin films attached to glass, New Journal of Chemistry 20 (1996) 233–241.
[11] Y.D. Hou, X.C. Wang, L. Wu, et al., Efficient decomposition of benzene over a β-Ga_2O_3 photocatalyst under ambient conditions, Environmental Science & Technology 40 (2006) 5799–5803.
[12] Z.H. Li, Z.P. Xie, Y.F. Zhang, et al., Wide band gap p-block metal oxyhydroxide InOOH: a new durable photocatalyst for benzene degradation, Journal of Physical Chemistry C 111 (2007) 18348–18352.
[13] H. Xue, Z.H. Li, L. Wu, et al., Nanocrystalline ternary wide band gap p-block metal semiconductor $Sr_2Sb_2O_7$: hydrothermal syntheses and photocatalytic benzene degradation, Journal of Physical Chemistry C 112 (2008) 5850–5855.
[14] J.H. Huang, X.C. Wang, Y.D. Hou, et al., Degradation of benzene over a zinc germanate photocatalyst under ambient conditions, Environmental Science and Technology 42 (2008) 7387–7391.
[15] X.N. Zhang, J.H. Huang, K.N. Ding, et al., Photocatalytic decomposition of benzene by porous nanocrystalline $ZnGa_2O_4$ with a high surface area, Environmental Science and Technology 43 (2009) 5947–5951.
[16] J.H. Huang, K.N. Ding, X.C. Wang, et al., Nanostructuring cadmium germanate catalysts for photocatalytic oxidation of benzene at ambient conditions, Langmuir 25 (2009) 8313–8319.
[17] C.S. Pan, Y.F. Zhu, New type of $BiPO_4$ oxy-acid salt photocatalyst with high photocatalytic activity on degradation of dye, Environmental Science and Technology 44 (2010) 5570–5574.
[18] C.S. Pan, Y.F. Zhu, Size-controlled synthesis of $BiPO_4$ nanocrystals for enhanced photocatalytic performance, Journal of Materials Chemistry 21 (2011) 4235–4241.
[19] C.S. Pan, D. Li, X.G. Ma, et al., Effects of distortion of PO_4 tetrahedron on the photocatalytic performances of $BiPO_4$, Catalysis Science and Technology 1 (2011) 1399–1405.
[20] G.F. Li, Y. Ding, Y.F. Zhang, et al., Microwave synthesis of $BiPO_4$ nanostructures and their morphology-dependent photocatalytic performances, Journal of Colloid and Interface Science 363 (2011) 497–503.
[21] C.S. Pan, J. Xu, Y. Chen, et al., Influence of OH-related defects on the performances of $BiPO_4$ photocatalyst for the degradation of rhodamine B, Applied Catalysis B: Environmental 115–116 (2012) 314–319.
[22] B. Lu, X.G. Ma, C.S. Pan, et al., Photocatalytic and photoelectrochemical properties of in situ carbon hybridized $BiPO_4$ films, Applied Catalysis A: General (2012).
[23] M. Long, W.M. Cai, J. Cai, et al., Efficient photocatalytic degradation of phenol over $Co_3O_4/BiVO_4$ composite under visible light irradiation, Journal of Physical Chemistry B 110 (2006) 20211–20216.
[24] A. Ishikawa, T. Takata, T. Matsumura, et al., Oxysulfides $Ln_2Ti_2S_2O_5$ as stable photocatalysts for water oxidation and reduction under visible-light irradiation, Journal of Physical Chemistry B 108 (2004) 2637–2642.
[25] H. Kato, K. Asakura, A. Kudo, Highly efficient water splitting into H_2 and O_2 over lanthanum-doped $NaTaO_3$ photocatalysts with high crystallinity and surface nanostructure, Journal of the American Chemical Society 125 (2003) 3082–3089.